Article

Law of Mechanical Properties of Full-Length Bonded Prestressed Bolts Influenced by Design Parameters

Fulu Shang [1], Xuchun Wang [1], Zhen Zhu [1,*], Peng Zhang [1], Mingqing Du [1], Ke Yu [2], Changfeng Yuan [1] and Xiaoming Guan [1]

[1]   School of Civil Engineering, Qingdao University of Techknowedge, Qingdao 266520, China
[2]   The Fourth Construction Co., Ltd. of China Construction Eighth Engineering Division, Qingdao 266100, China
*   Correspondence: zhuzhen@qut.edu.cn

Abstract: Design parameters such as initial bonding section, prestress, and bonding stiffness have a significant impact on the mechanical properties of the full-length bonded prestressed bolt. In order to understand the influence of the above three parameters on the axial force and shear stress of anchor bolts under the condition of rock separation, theoretical and numerical models were established, and the sensitivity of different parameters was analyzed based on the grey correlation method. Results indicate that the bonding stiffness had the greatest impact on the mechanical properties of the bolt and largely determined the peak axial force, peak interfacial shear stress, and number of sliding elements. Moreover, prestress had a significant impact on the peak axial force and the distribution of shear stress in the initial bonding section, while the length of the initial bonding section had a significant impact on the number of sliding elements and the peak axial force after sliding. The grey correlation method results show that the correlation degrees of the initial bonding section, prestress, and bonding stiffness were 0.8932, 0.9023, and 0.9775, respectively.

Keywords: full-length bonded; full-length bonded prestressed bolts; bond stiffness; bed separation; grey relational analysis

1. Introduction

As a simple and economic support structure, bolts account for more than 80% of roadway support [1]. In recent years, many new types of bolts have emerged such as basalt fiber composite bolt, GFRP bolt, NPR bolt, new tension dispersing twist bolt, and so on [2–7]. According to the length of anchorage, the bolt support system is mainly divided into end anchorage, lengthened anchorage, and full-length anchorage [8]. Compared with end anchorage and lengthened anchorage, the support effect of full-length anchorage is more advantageous [9]. The stress and strain of the full-length bonded bolts are not evenly distributed along the length direction of the bolt, and the bolt has great stress in the part with a large fracture aperture, so the stress of the bolt body is very sensitive to surrounding rock deformation and separation, which can timely suppress the surrounding rock separation and sliding, and the support stiffness is high [10]. As a type of full-length anchorage bolt, the full-length bonded prestressed bolt has the advantages of both the end-anchored prestressed bolt and full-length bonded unprestressed bolt, and has been used more and more widely in support engineering.

The research methods of full-length anchoring bolts mainly include theoretical calculations, laboratory and field test research, and numerical simulations. Wei Sijiang [11] believed that the pretightening force of a full-length bonded bolt was one of the factors affecting the strength characteristics of the anchorage body, and finally concluded that adding the pretightening force could improve the bearing capacity of the anchoring system through test and on-site verification. Huang Minghua [12] analyzed the mechanical characteristics of the full-length bonded unprestressed bolt under the action of rock mass separation in the

full-course, and believed that the fracture position had a great influence on the mechanical characteristics of the bolt. Zheng Xuanrong [13] derived the stress distribution law in the anchoring zone formed by the full-length bonded prestressed bolt under the pretightening force based on the action mechanism of a single full-length bonded prestressed bolt in surrounding rock. Based on the shear slip model of the anchorage interface under the action of drawing, Ding Xiao [14] derived the formula of the bolt axial force and interface shear stress in elastic and elastic–plastic states under the action of single bed separation by approximating the fracture aperture as the sum of shear displacements of the anchorage interface on the left and right sides of the bed separation, and analyzed the full-range mechanical characteristics of the bolt under bed separation. C. Li and B. Stolborg [15] studied the mechanical characteristics of bolts in the jointed rock mass and found that the axial force and interface shear stress of the bolt on both sides of the crack distributed symmetrically when the anchorage length was large enough, and the anchorage interface would strip first at the crack with the development of the crack. Das [16] established a bolt reinforcement model for the full-length anchoring of a circular surrounding rock roadway with a single fissure based on the elastic hypothesis, and deduced the expressions of the bolt deformation, axial force, and shear under the condition of single fissure opening. Li Jianjian [17] compared the distribution characteristics of axial force and shear stress of the bolt under the condition of full-length anchorage and end anchorage, and believed that the distribution characteristics of bearing capacity of the bolt were closely related to anchorage conditions, prestress, the diameter of the bolt, and the strength of the surrounding rock. In addition, many scholars have carried out a lot of research by using numerical simulation methods and achieved fruitful results [18–21].

There are two problems in the above research. (1) In the theoretical calculation and numerical simulations, there has been more research on the full-length bonded non-prestressed bolt, but less research on the full-length bonded prestressed bolt. (2) The research results related to the full-length bonded prestressed anchor bolt have mainly focused on the influence of the separation layer and rock mass properties on the anchoring performance, while the influence of design parameters on the anchoring performance under the separation condition is less involved. To further explore the mechanical properties of the full-length bonded prestressed bolts under the influence of design parameters under the condition of separation, based on the existing research results, the mechanical calculation model of the full-length bonded prestressed bolt was established in this paper, and the influence law of three-bolt parameters on the mechanical properties of the bolt was revealed by the verified numerical simulation method, which provides a theoretical basis for the design of a full-length bonded prestressed bolt. A systematic study of the influence of design parameters on the mechanical characteristics of the full-length bonded prestressed bolts is helpful to understand the action mode and failure behavior of full-length bonded prestressed bolts under laying-off conditions and to guide the support design.

2. Basic Structure and Theoretical Model of the Bolt

2.1. Basic Structure

Rock bolting mainly uses the bolt to reinforce the surrounding rock mass of the roadway so that the bolt and the rock mass within the anchoring range together form a support system to support the roadway roof [22]. The ideal full-length bonded prestressed bolt should be implemented in two steps: first, the prestress is applied through the end anchorage, and then the full-length bonded bolt is realized, and the implementation process of the full-length bonded bolt will not interfere with the tensile process of the bolt [23,24]. Figure 1 shows the basic components of the full-length bonded prestressed bolt: the whole bolt body is bonded to the bolt hole wall, which can be divided into the initial bonding section (L_d) and the second bonding section (L_a) according to the sequence of anchor grout condensation. The initial bonding section is used to apply the prestress to the bolt, and the second bonding section realizes the full-length bonding of the bolt after the prestress is applied.
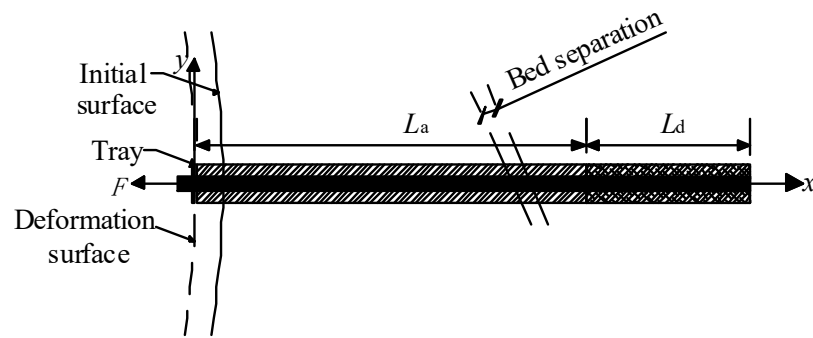
Figure 1. Basic constitution of the full-grouted prestressed bolt.

Since the application of prestress and full-length bonding are implemented separately, the mechanical model (Figure 2a) of a full-length bonded prestressed bolt under the action of a separation layer can be regarded as the superposition of the end-anchored prestressed bolt model (Figure 2b) and the full-length bonded unprestressed bolt model (Figure 2c) under the action of the crack.
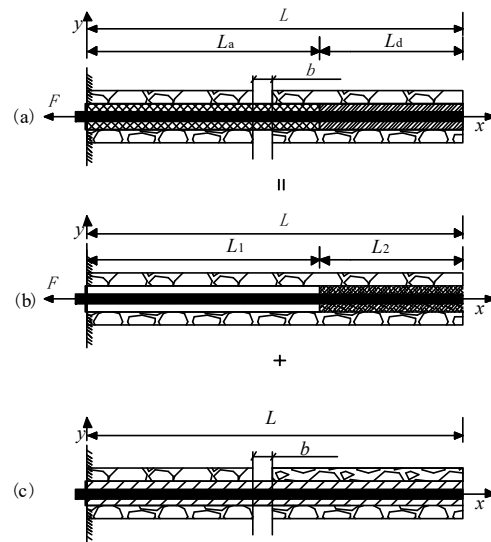
Figure 2. Analytical model of the full-length bonded prestressed bolts. (**a**) full-length bonded prestressed bolt; (**b**) end-anchored prestressed bolt; (**c**) full-length bonded unprestressed bolt.

Here, F is the tension on the bolt; L is the total length of the bolt; L_d is the length of the initial bonding section; L_a is the length of the secondary bonded segment, where the initial bonding section is used to apply to prestress to the bolt, and the secondary bonding section is used to achieve the full-length bonding of the bolt; L_1 is the length of the free section; L_1 is the length of the anchorage section; b is the size of the bed separation.

2.2. Theoretical Model

Studies [25] have shown that under the action of prestress, the expressions of the axial force and the shear stress of full-length bonded prestressed bolts in an elastic state are as follows:

$$P(x) = \begin{cases} Q & 0 \le x \le L_1 \\ \dfrac{Q\,\text{sh}[\beta(L-x)]}{\text{sh}(\beta L_2)} & L_1 \le x \le L_2 \end{cases} \tag{1}$$

$$\tau(x) = \begin{cases} 0 & 0 \leq x \leq L_1 \\[2mm] \dfrac{\beta Q \mathrm{ch}[\beta(L-x)]}{\pi D \mathrm{sh}(\beta L_2)} & L_1 \leq x \leq L_2 \end{cases} \tag{2}$$

where Q is the prestress imposed on the bolt; x is the distance from the right end of the bolt; β is the coefficient related to the bolt and surrounding rock, $\beta = \sqrt{4K/(\pi D^2 E_a)}$; K is the shear stiffness coefficient of the surrounding rock; E_a is the composite elastic modulus, $E_a = \frac{E_g(D^2-d^2)+E_b d^2}{D^2}$; E_b is the elastic modulus of the bolt; E_g is the elastic modulus of slurry; d is the diameter of the bolt; D is the diameter of the anchor solid.

According to the shear slip theory of anchorage interface under the tensile force, the bed separation value can be regarded as the sum of the relative displacements between the anchor solid and surrounding rock on the left and right sides of the bed separation [8]. As shown in Figure 3, the anchor solid micro-segments with length dx are taken on both sides of the crack. According to static equilibrium conditions and Hooke's Law:

$$\frac{du(x)}{dx} = -\frac{4P(x)}{\pi D^2 E_a} \tag{3}$$

$$\frac{dP(x)}{dx} = -\pi D \tau(x) \tag{4}$$

where x_0 is the distance between the separation position and left end of the bolt.
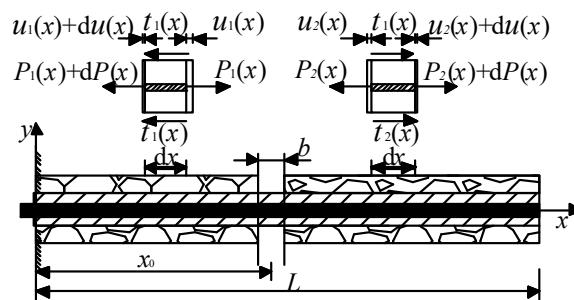
Figure 3. Static equilibrium of the anchorage micro-segment.

In combination with Equations (3) and (4), we get:

$$\frac{d^2(u)}{dx^2} - \frac{4\tau(u)}{DE_a} = 0 \tag{5}$$

where $\tau(u)$ is the lateral resistance on the hole wall, which is a function of shear displacement u, $\tau(u) = Ku$ in the elastic state, and K is the shear stiffness coefficient.

By solving Equation (5), the stress distribution expression on both sides of the bed separation can be obtained:

Left:

$$\tau_1(x) = \frac{\beta^2 E_a D \mathrm{ch}(\beta x)}{4\omega \mathrm{sh}(\beta x_0)} b \tag{6}$$

$$P_1(x) = \frac{\pi D^2 \beta E_a \mathrm{sh}(\beta x)}{4\omega \mathrm{sh}(\beta x_0)} b \tag{7}$$

Right:

$$\tau_2(x) = \frac{\beta^2 E_a D \mathrm{ch}[\beta(L-x)]}{4\omega \mathrm{sh}[\beta(L-x_0)]} b \tag{8}$$

$$P_2(x) = \frac{\pi D^2 \beta E_a \text{sh}[\beta(L-x)]}{4\omega \text{sh}[\beta(L-x_0)]} b \tag{9}$$

where $\omega = \{\coth(\beta x_0) + \coth[\beta(L-x_0)]\}$.

According to the theoretical model (Figure 2) and the superposition principle, the expressions of the axial force and the shear stress of the full-length bonded prestressed bolts under the bed separation in the elastic state can be obtained by connecting Equations (1), (2), (6)–(9):

When $x \leq x_0$,

$$P(x) = \frac{\pi D^2 \beta E_a \text{sh}(\beta x)}{4\omega \text{sh}(\beta x_0)} b + Q \tag{10}$$

$$\tau(x) = \frac{\beta^2 E_a D \text{ch}(\beta x)}{4\omega \text{sh}(\beta x_0)} b \tag{11}$$

When $x_0 < x \leq L_a$,

$$P(x) = \frac{\pi D^2 \beta E_a \text{sh}[\beta(L-x)]}{4\omega \text{sh}[\beta(L-x_0)]} b + Q \tag{12}$$

$$\tau(x) = \frac{\beta^2 E_a D \text{ch}[\beta(L-x)]}{4\omega \text{sh}[\beta(L-x_0)]} b \tag{13}$$

When $L_a < x \leq L$,

$$P(x) = \frac{\pi D^2 \beta E_a \text{sh}[\beta(L-x)]}{4\omega \text{sh}[\beta(L-x_0)]} b + \frac{Q \text{sh}[\beta(L-x)]}{\text{sh}(\beta L_d)} \tag{14}$$

$$\tau(x) = \frac{\beta^2 E_a D \text{ch}[\beta(L-x)]}{4\omega \text{sh}[\beta(L-x_0)]} b + \frac{\beta Q \text{ch}[\beta(L-x)]}{\pi D \text{sh}(\beta L_d)} \tag{15}$$

3. Numerical Model Establishment and Feasibility Verification

3.1. Numerical Model

The model was composed of two blocks with the side length of 1 m, and cracks were set between the blocks. The separation of blocks was used to simulate the rock mass separation. The length of the bolt was 1.8 m, which was divided into 18 segments. The right end boundary of the model was fixed, as shown in Figure 4. The model parameter values are shown in Table 1 [21].

Table 1. The model parameters.

Object	Parameters	Value
Block	Constitutive model	Elastic
	Elasticity modulus/GPa	50
	Poisson's ratio	0.2
	Density/(kg·m^{-3})	2500
Bolt	Elasticity modulus/GPa	200
	Cohesion force/(10^6N·m^{-1})	1.0
	Bond stiffness/GPa	1.0
	Strength of extension/kN	500
	Internal friction angle/°	30
	Diameter/mm	20
Tray	Elasticity modulus/GPa	25
	Poisson's ratio	0.15

The FISH language was used to develop the progressive slip failure algorithm of the bolt under bed separation. When the sheer force of the anchoring interface reaches the

defined cohesion force of the anchoring interface, which begins to slip, the cohesion force and bond stiffness of the bolt element is re-assigned to 0. To obtain the anchor progressive damage, the algorithm will be implemented in each calculation step. The FISH language was used to develop the progressive slip failure algorithm of the bolt under bed separation, as shown in Appendix A.
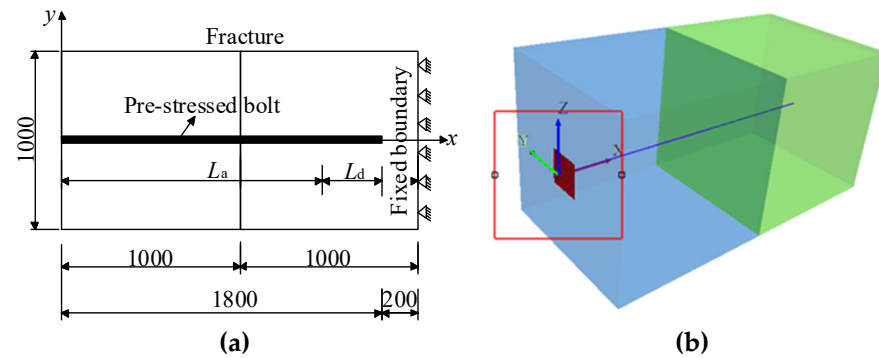
Figure 4. Numerical model. (**a**) Model parameter; (**b**) 3D model.

3.2. Feasibility Verification of Numerical Model

To verify the rationality of the above numerical model, the bed separation value was 2 mm, L_a was 400 mm, and the prestress was 40 kN. The theoretical calculation and numerical simulation analysis were carried out respectively. The axial force and anchoring interface shear stress of full-length bonded prestressed bolt were compared, as shown in Figure 5. The two blocks of the model had a displacement of 2 mm in the bed separation, which caused the bolt to be stretched to both sides at the separation layer. Therefore, the peak of the bolt axial force at the separation layer was close to 300 kN in Figure 5a. Corresponding to the change in the axial force of the bolt, the shear stress value at the anchorage interface showed an inverse sign on both sides of the bed separation. Therefore, in Figure 5b, the shear stress at the anchorage interface peaked close to 15 MPa on both sides of the bed separation. As can be seen in Figure 5a, the axial force of the bolt on the left side of the separation layer gradually decayed to the initial prestress applied, and the axial force of the bolt on the right side of the separation layer gradually decayed to zero. As can be seen in Figure 5b, the shear stress at the anchorage interface on the left side of the separation layer gradually decayed to zero, while the shear stress at the anchorage interface on the right side of the separation layer first decreased, then increased, and then decreased due to the effect of the initial prestress.
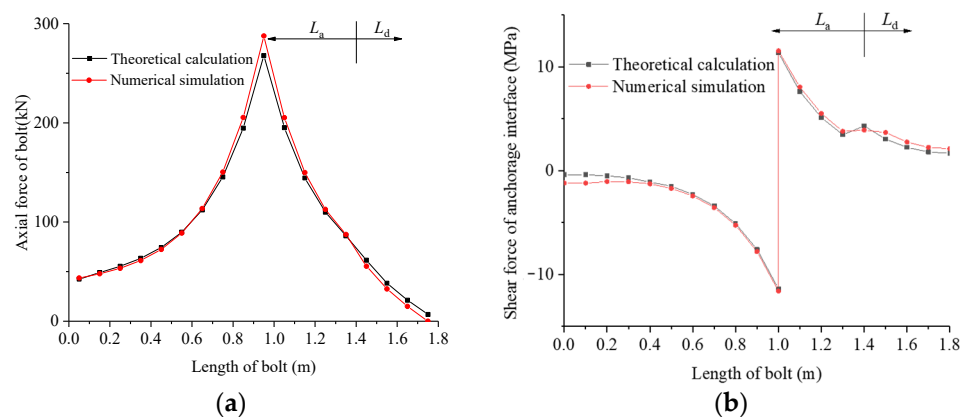
Figure 5. Comparison between the numerical simulation and theoretical analysis. (**a**) Axial force of the bolt. (**b**) Shear force of the anchorage interface.

The comparison results show that the theoretical calculation results were in good agreement with the numerical simulation results, which indicates that the numerical analysis method is feasible.

4. Analysis of Influence of Design Parameters on the Mechanical Characteristics of the Bolt

4.1. Mechanics Characteristics of the Bolt under Different L_d

The prestress of the bolt was set to 40 kN, the bed separation value was set to 2 mm and 4 mm, and L_d was set to 400 mm, 600 mm, 800 mm, and 900 mm, respectively. The numerical model test was carried out, and the test results are shown in Figure 6. It can be seen in Figure 6a that when the fracture aperture was 2 mm, the axial force variation in the bolt was consistent, and the bolt did not slip. The axial force of the bolt reached the maximum value at the separation layer, and the maximum value was almost the same. When the fracture opened to 4 mm, the bolts all started to slide, and the "axial force platform" (i.e., the interval with the same axial force) appeared. When the L_d was 400 mm, there were two sliding elements; when L_d was 600 mm, 800 mm, and 900 mm, there were three sliding elements. Due to the increase in the sliding elements, when L_d was 600 mm, 800 mm, and 900 mm, the maximum axial force of the bolt at the bed separation was smaller than that when the L_d was 400 mm. As can be seen in Figure 6b, the shear stress at the anchorage interface reached its peak at the fracture, and the shear stress signs on both sides of the separation layer were the opposite. When the fracture aperture was 2 mm and L_d was 400 mm, the shear stress of the anchorage interface increased first and then decreased on L_a. When L_d was 600 mm, 800 mm, and 900 mm, the shear stress variation in the anchorage interface was consistent on L_d. When the fracture aperture was 4 mm, the shear stress of the anchorage interface showed a zero interval, corresponding to the "axial force platform" of the bolt.
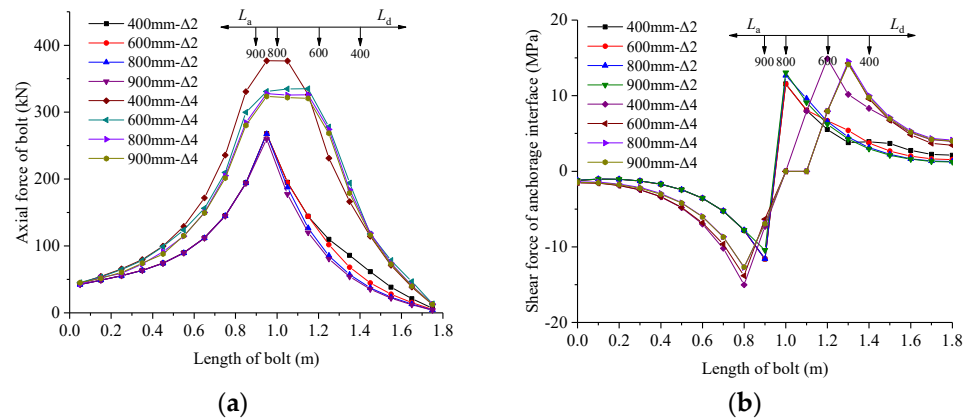
Figure 6. Simulation results of different values of L_a. (**a**) Axial force of the bolt. (**b**) Shear force of the anchorage interface.

When the value of the bed separation was 4 mm, the axial displacement cloud map of the bolt and the anchoring agent displacement cloud map corresponding to different L_a values were as shown in Figures 7 and 8. It can be seen from Figure 7 that when the L_a was different, the axial displacement of the bolt changed in the same law: the axial displacement of the bolt gradually increased from the right end to the left end, while the leftmost end of the anchor bolt gradually decreased due to the influence of the tray. It can be seen from Figure 8 that when L_a was different, the displacement of the anchoring agent also changed in the same law: the displacement of the anchoring agent on both sides of the bed separation was the largest, and the displacement of the anchoring agent gradually decreased from the separation layer to both ends, and the displacement at the leftmost end of the bolt increased again due to the action of the tray. The variation laws of axial displacement of the bolt and the anchoring agent confirm the variation laws in the axial force and shear stress in Figure 6. With the increase in L_a, the maximum axial displacement

of the bolt decreased gradually, the maximum reduction was 6%, and the change in the anchoring agent displacement was not obvious, which indicates that the initial bond length can limit the displacement of the bolt to a certain extent.
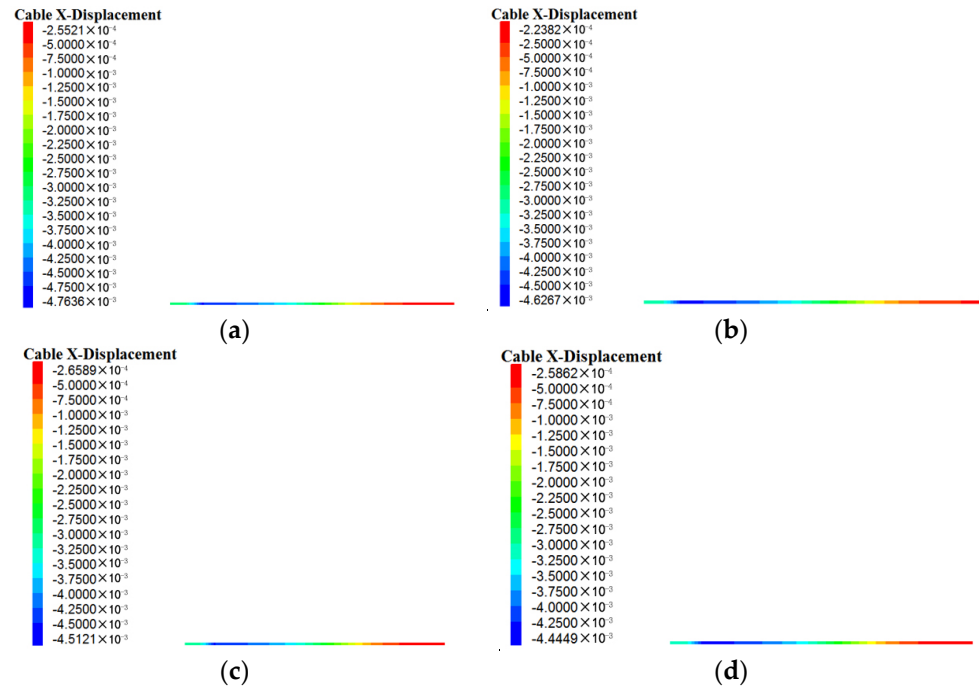
Figure 7. Cloud image of the cable displacement under different L_a (with a fracture aperture of 4 mm). (**a**) L_a = 400 mm; (**b**) L_a = 600 mm; (**c**) L_a = 800 mm; (**d**) L_a = 900 mm.
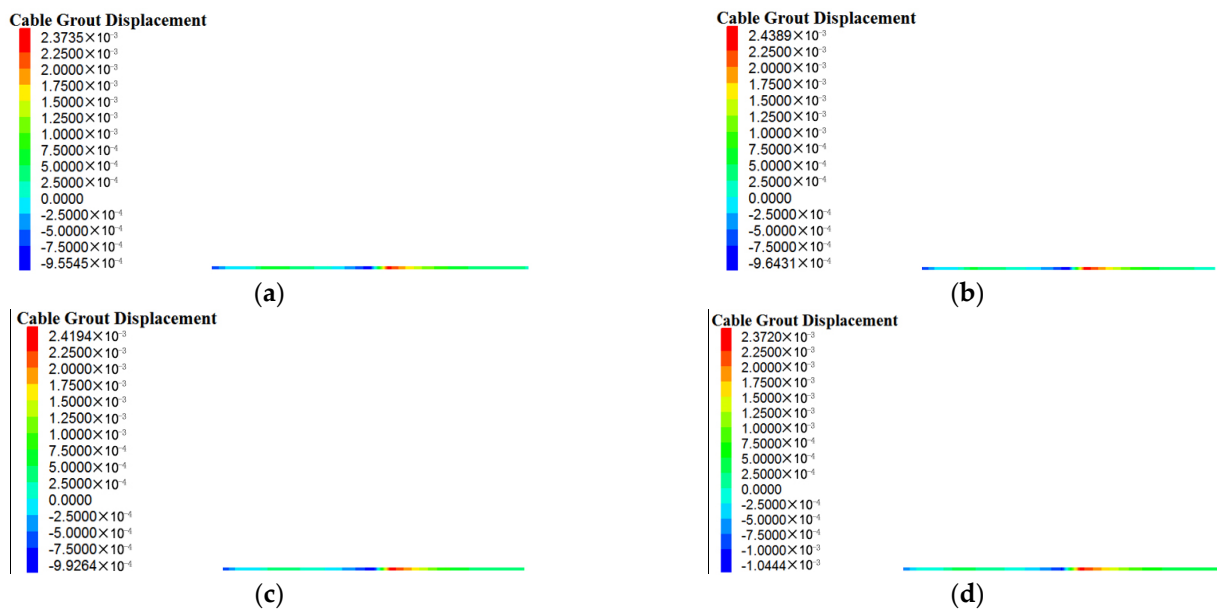
Figure 8. Cloud image of the cable grout displacement under different L_a (with a fracture aperture of 4 mm). (**a**) L_a = 400 mm; (**b**) L_a = 600 mm; (**c**) L_a = 800 mm; (**d**) L_a = 900 mm.

4.2. Mechanics Characteristics of the Bolt under Different Sizes of Prestress

L_a was set at 400 mm, the bed separation value was set at 2 mm and 4 mm, and the prestress was set at 20 kN, 40 kN, 60 kN, and 80 kN, respectively. The numerical model test was carried out, and the test results are shown in Figure 9. It can be seen from Figure 9a that the axial force of the bolt followed the same change rule under different prestresses,

and the maximum value appeared at the separation layer. Under the bed separation, the maximum axial force of the bolt increased with the increase in prestress. It can be seen from Figure 9b that the shear stress at the anchorage interface reached its peak at the separation layer, and the shear stress signs on both sides of the separation layer were the opposite. The larger the bed separation value, the greater the peak value of the shear stress on the anchorage interface. When the fracture aperture was 2 mm, the shear stress curves of the anchorage interface overlapped on L_b. On L_a, the shear stress of the anchorage interface increased first and then decreased when the prestress was 80 kN and 60 kN, and showed a decreasing trend when the prestress was 40 kN and 20 kN. When the crack was 4 mm wide, the shear stress curves of the anchorage interface overlapped on L_b. On L_a, the shear stress of the anchorage interface all showed a decreasing trend.
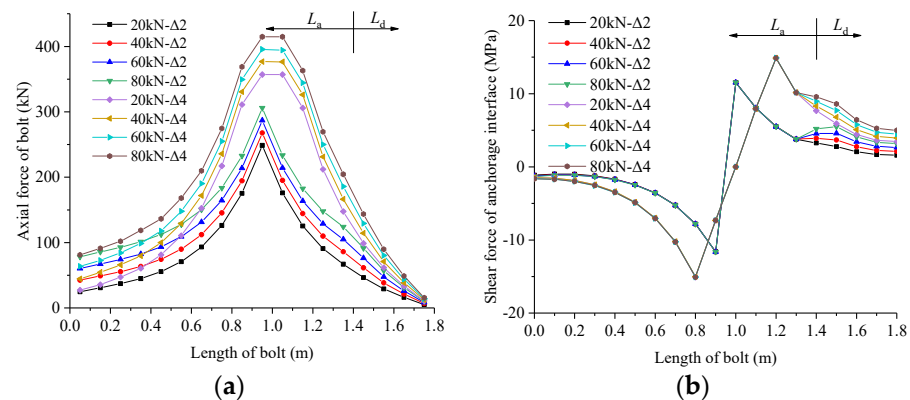
Figure 9. Simulation results of the different sizes of prestress. (**a**) Axial force of the bolt. (**b**) Shear force of the anchorage interface.

When the value of the bed separation was 4 mm, the axial displacement cloud map of the bolt and the anchoring agent displacement cloud map corresponding to different L_a values were as shown in Figures 10 and 11. It can be seen from Figure 10 that when the prestress was different, the axial displacement of the bolt changed in the same law: the axial displacement of the anchor bolt gradually increased from the right end to the left end, while the leftmost end of anchor bolt gradually decreased due to the influence of the tray. It can be seen from Figure 11 that when the prestress was different, the displacement of the anchoring agent changed in the same law: the displacement of the anchoring agent on both sides of the bed separation was the largest, and the displacement of the anchoring agent gradually decreased from the separation layer to both ends, and the displacement at the leftmost end of the bolt increased again due to the action of the tray. The variation laws of the axial displacement of the bolt and the anchoring agent confirm the variation laws of the axial force and shear stress in Figure 9. With the increase in the prestress, the maximum axial displacement of the bolt increased by 31%, and the maximum displacement of the anchorage grout increased by 28.2%, which indicates that the prestress has a significant effect on the axial displacement of the bolt.

4.3. Mechanics Characteristics of Bolt under Different Bond Stiffness

L_a was set at 400 mm, the prestress was set at 40 kN, the bed separation value was set at 2 mm and 4 mm, and the bond stiffness was set at 0.6 GPa, 0.8 GPa, 1.0 GPa, 1.2 GPa, and 1.4 GPa, respectively. The numerical model test was carried out, and the test results are shown in Figure 12. It can be seen from Figure 12a that when the fracture aperture was 2 mm, the bolt axial force reached its peak value at the separation layer, and the bolt axial force increased with the increase in the bond stiffness, and the overall change law was consistent. When the crack was 4 mm wide and the bond stiffness was 0.6 GPa and 0.8 GPa, there was no sliding failure element in the bolt. The bond stiffness was 1.0 GPa, 1.2 GPa, and 1.4 GPa, and the bolt had 2, 3, and 4 slip failure units, respectively. It can be seen from Figure 12b that the shear stress at the anchorage interface reached its peak at the

separation layer, and the values of shear stress on both sides of the separation layer were the opposite. When the bond stiffness was different, the shear stress on the whole bolt kept the same change rule. The peak value of shear stress on the anchorage interface increased with the increase in the bond stiffness. The peak values of shear stress were the same when the bond stiffness was different. The shear stress at the anchorage interface appeared as a zero value interval corresponding to the "axial force platform", which was consistent with the change law of the axial force.
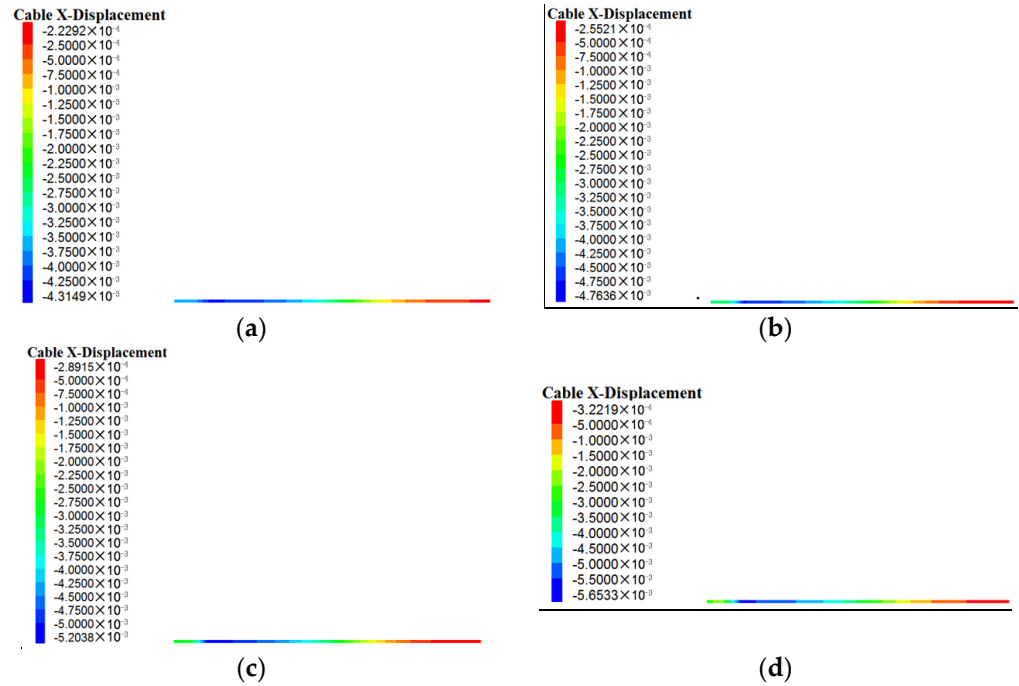
Figure 10. Cloud image of the cable displacement under different prestress (with fracture aperture of 4 mm). (**a**) Prestress = 20 kN; (**b**) prestress = 40 kN; (**c**) prestress = 60 kN; (**d**) prestress = 80 kN.
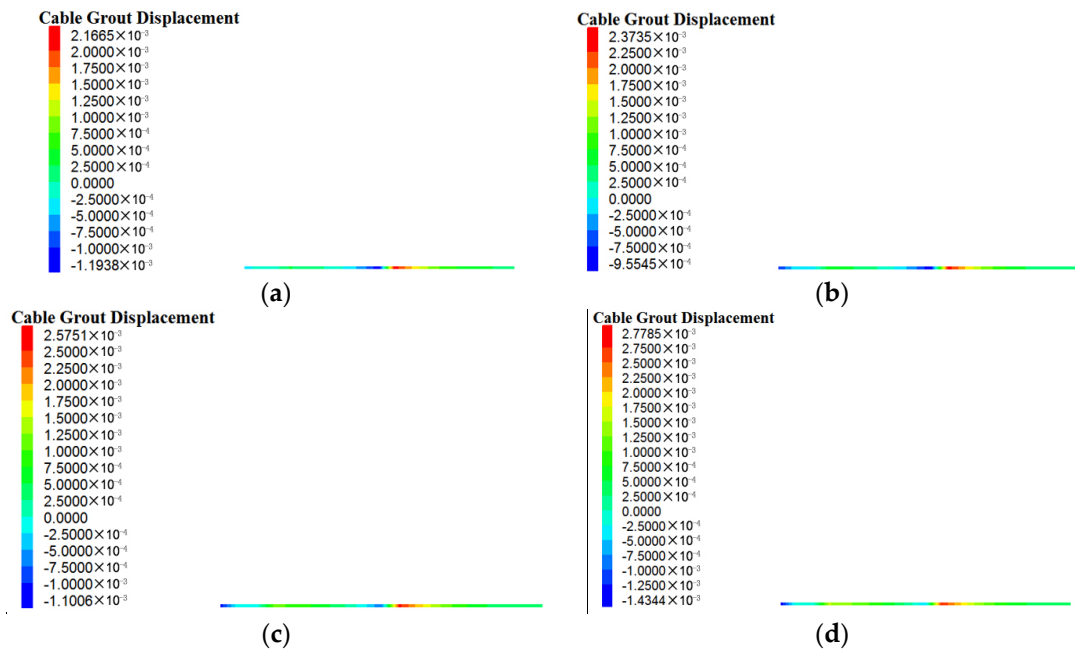
Figure 11. Cloud image of the cable grout displacement under different prestress (with fracture aperture of 4 mm). (**a**) Prestress = 20 kN; (**b**) prestress = 40 kN; (**c**) prestress = 60 kN; (**d**) prestress = 80 kN.
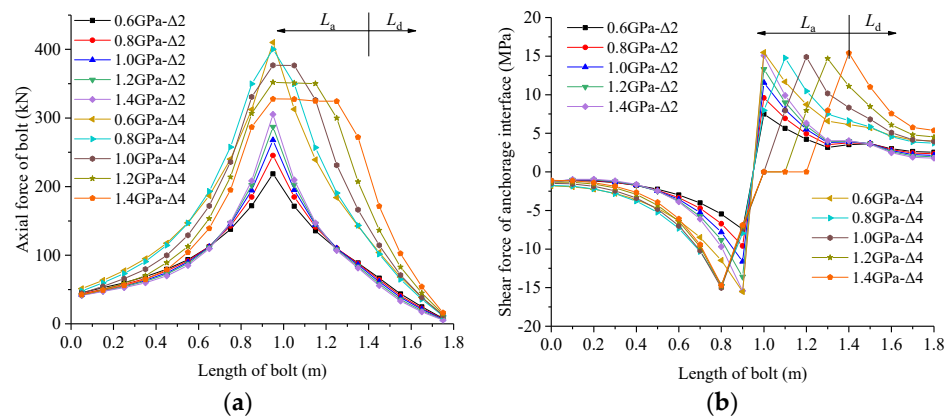
Figure 12. Simulation results of the different bond stiffness. (**a**) Axial force of the bolt. (**b**) Shear force of the anchorage interface.

When the value of the bed separation was 4 mm, the axial displacement cloud map of the bolt and the anchoring agent displacement cloud map corresponding to different bond stiffness were as shown in Figures 13 and 14. It can be seen from Figure 13 that when the bond stiffness was different, the axial displacement of the bolt changed in the same law: the axial displacement of the bolt gradually increased from the right end to the left end, while the leftmost end of the bolt decreased gradually due to the influence of the tray. It can be seen from Figure 14 that when the bond stiffness was different, the displacement of the anchoring agent changed in the same law: the displacement of the anchoring agent on both sides of the separation layer was the largest, and the displacement of anchoring grout gradually decreased from the separation layer to both ends, and the displacement at the leftmost end of the bolt increased again due to the action of the tray. The variation laws of the axial displacement of the bolt and the anchoring agent confirm the variation laws of axial force and shear stress in Figure 12. With the increase in the bond stiffness, the maximum axial displacement of the bolt increased by 1.5%, and the maximum displacement of the anchoring agent increased by 32.4%, which indicates that bond stiffness has a significant effect on the displacement of anchor grout.

Figure 13. *Cont.*

(**e**)
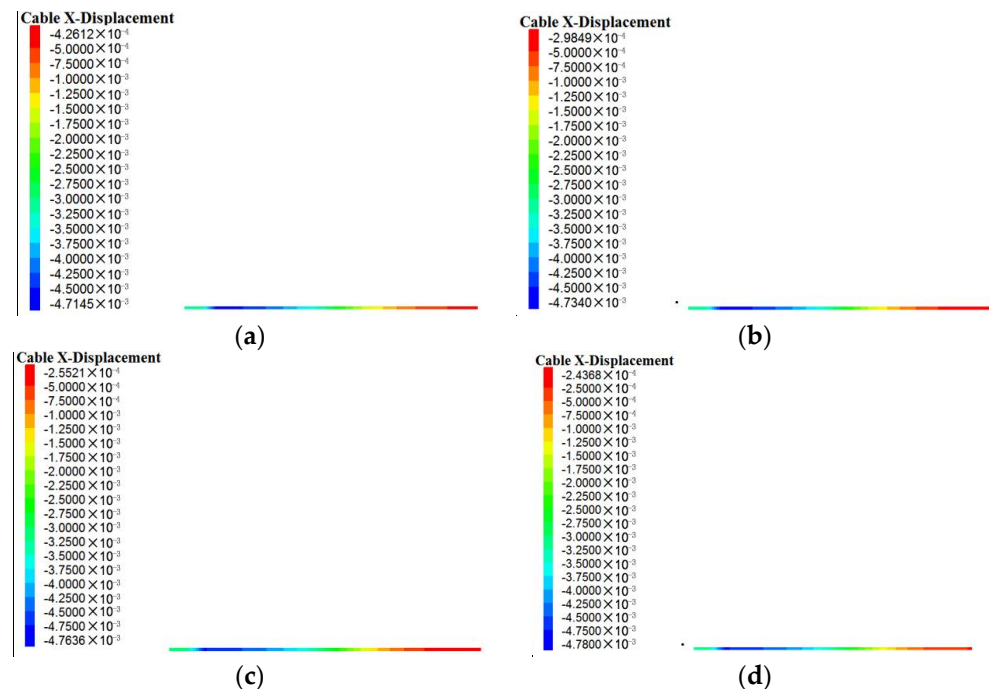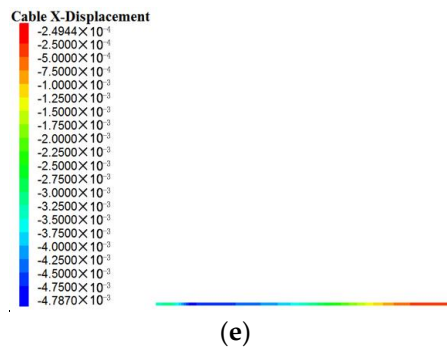
Figure 13. Cloud image of the cable displacement under different bond stiffness (with a fracture aperture of 4 mm). (**a**) Bond stiffness = 0.6 GPa; (**b**) bond stiffness = 0.8 GPa; (**c**) bond stiffness = 1.0 GPa; (**d**) bond stiffness = 1.2 GPa; (**e**) bond stiffness = 1.4 GPa.
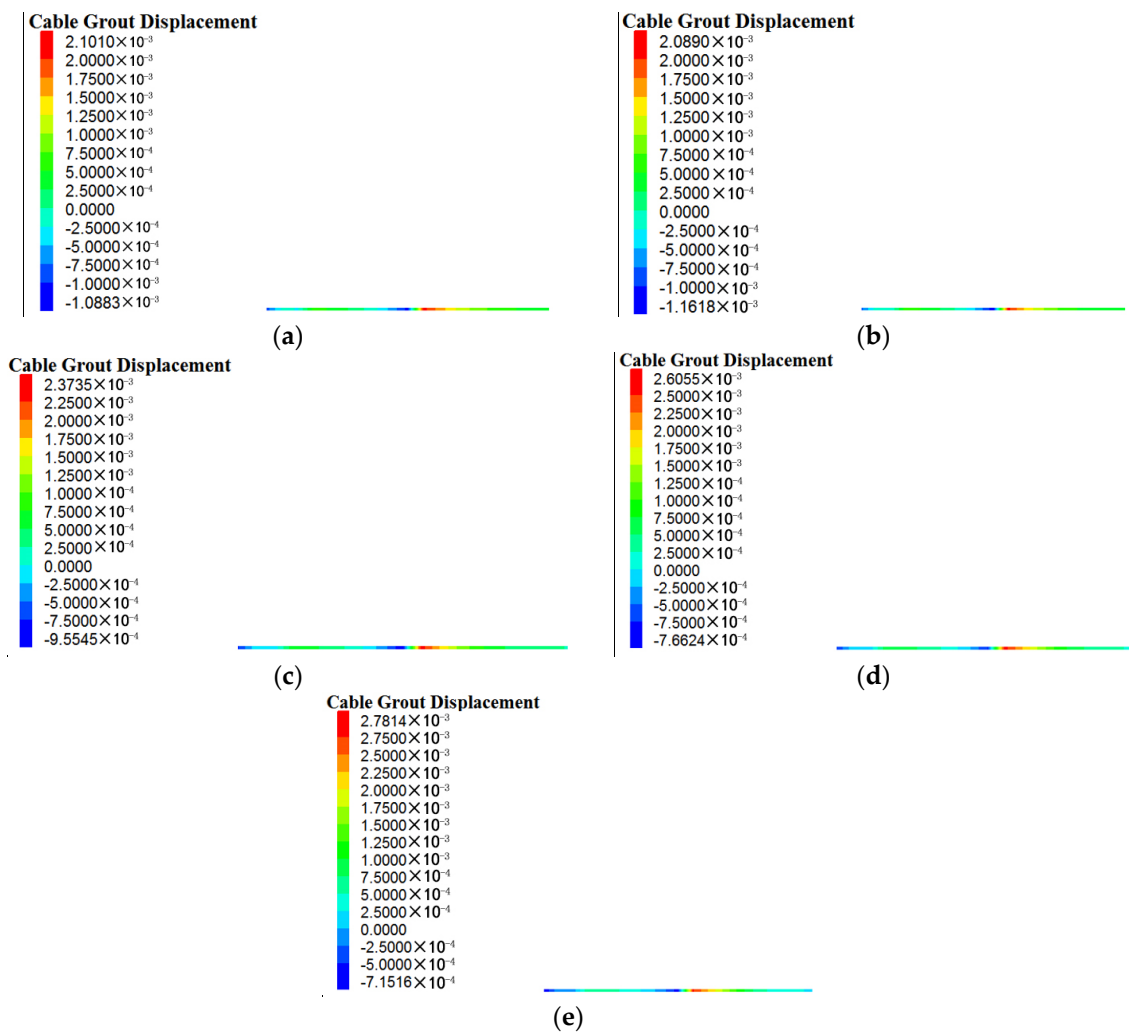
Figure 14. Cloud image of the cable grout displacement under different bond stiffness (with fracture aperture of 4 mm). (**a**) Bond stiffness = 0.6 GPa; (**b**) bond stiffness = 0.8 GPa; (**c**) bond stiffness = 1.0 GPa; (**d**) bond stiffness = 1.2 GPa; (**e**) bond stiffness = 1.4 GPa.

5. Sensitivity Analysis of Design Parameters

Based on the above analysis, the length of the initial bond section and prestress and bond stiffness can all produce different effects on the mechanical properties of the bolt. To study the influence of various factors on the mechanical properties of bolts, the Grey correlation method was used to analyze the sensitivity of three design parameters by

taking the sliding element number as the evaluation index. Table 2 shows the orthogonal experimental parameters at L$_9$(3^4). The number of sliding elements in nine orthogonal tests was 0, 2, 3, 4, 0, 4, 3, 4, 0, respectively.

Table 2. The orthogonal test parameters.

Serial Number	Initial Bond Section (mm)	Size of Prestress (kN)	Bond Stiffness (GPa)
E1	400	40	0.6
E2	400	60	1
E3	400	80	1.2
E4	600	40	1.2
E5	600	60	0.6
E6	600	80	1
E7	800	40	1
E8	800	60	1.2
E9	800	80	0.6

The implementation of Grey correlation analysis can be divided into four steps [26,27]. First, the data in Table 2 were mean-averaged and dimensionless according to Equation (16), and the processing results are shown in Table 3. Second, the correlation coefficient was calculated according to Equation (17). Then, the correlation degree was calculated according to Equation (18), and the calculation results are shown in Table 4. Finally, the correlation degree of each parameter was sorted.

$$X_i(k) = \frac{x_i(k)}{\overline{x}_i}, i = 1, 2, \ldots, m, k = 1, 2, \ldots, N, \tag{16}$$

where $X_i(k)$ is the dimensionless mean value of the i influence parameter; i is the serial number of the impact parameter; k is the data serial number; x_i is the arithmetic mean value of $x_i(1), x_i(2), \ldots, x_i(N)$; m is the number of impaction parameters; N is the number of data.

$$\xi_i(k) = \frac{\displaystyle\min_i \min_k |X_0(k) - X_i(k)| + \rho \max_i \max_k |X_0(k) - X_i(k)|}{|X_0(k) - X_i(k)| + \rho \max_i \max_k |X_0(k) - X_i(k)|}, \tag{17}$$

where $\xi_i(k)$ is the Grey correlation coefficient of influencing factors; $X_0(k)$ is the dimensionless mean value of a reference sequence; $X_i(k)$ is the mean to dimensionless value of a comparison sequence; ρ is the resolution coefficient, which is 0.5.

$$\gamma_i = \frac{1}{N} \sum_{k=1}^{N} \xi_i(k), \tag{18}$$

where γ_i is the correlation degree of each impact factor.

Table 3. The orthogonal test data mean value dimensionless value.

Serial Number	Initial Bond Section (mm)	Size of Prestress (kN)	Bond Stiffness (GPa)	Sliding Elements Number
E1	0.6667	0.6667	0.6431	0
E2	0.6667	1.0000	1.0718	2
E3	0.6667	1.3333	1.2862	3
E4	1.0000	0.6667	1.2862	4
E5	1.0000	1.0000	0.6431	0
E6	1.0000	1.3333	1.0718	4
E7	1.3333	0.6667	1.0718	3
E8	1.3333	1.0000	1.2862	4
E9	1.3333	1.3333	0.6431	0

Table 4. The relevance data of each impact factor.

Parameter	Initial Bond Section	Size of Prestress	Bond Stiffness
Correlation degree	0.8932	0.9023	0.9775

According to the calculation results in Table 4, it can be seen that the influences of three bolt parameters on the mechanical properties of the bolts are sorted as follows: bond stiffness > prestress > initial bonding length. The correlation degree between the initial bonding length and the size of the prestress was approximately 0.9, and the correlation degree between the bond stiffness was approximately 1.0, indicating that the three factors were all main factors affecting the sliding failure of the bolt, and the bond stiffness had the greatest influence on the sliding failure of the bolt. According to the preceding paragraph, bond stiffness had a significant impact on the number of sliding elements, and the length of the initial bond section and the size of prestress were also influential factors on the number of sliding elements. Furthermore, there was little difference between the two sensitivity parameters, and the degree of influence on the number of sliding elements was similar.

6. Limitations and Further Research Plan

(1) The effect of the bed separation on the bolt is relatively complicated. Some bolts may be subjected to shear or eccentric tension. In this paper, only the bed separation perpendicular to the axial direction of the bolt was considered.

(2) In this paper, FLAC 3D software was used for the numerical simulation analysis, and the accuracy of the calculation results was not compared with other methods. Recently, more novel and stronger numerical methods have been proposed for the stress analysis of isotropic or anisotropic media. Among them, the "differential quadrature method" and the "Bessel method" have higher stability and accuracy than other numerical methods [28,29]. Using these methods, the influences of initial bond length, prestress size, and bond stiffness on the mechanical properties of the full-length bonded prestressed bolts can be determined "alternately".

(3) The mechanical parameters of bolt components selected in this paper refer to the parameters selected in the research work of Wang Xiaoqing et al. [21], and the main considerations were as follows. This paper focused on the influence of the bolt design parameters on the mechanical properties of the bolt under the action of stratification. To reduce the deformation of the block, a higher elastic modulus was selected. In this paper, the relative deformation of blocks was used to simulate the separation deformation, and the separation force caused by the deformation was much larger than that of the actual project. To better reveal the change law of the axial force and shear stress of the anchorage interface under the deformation of the separation layer, the mechanical parameter value of the bolt was larger than that of the actual project.

The above limitations can be further discussed and studied in the next step, especially the use of a numerical calculation method with higher stability and accuracy, which is more valuable and feasible.

In general, the initial bond segment and the secondary bond segment were defined for the first time in this paper. Based on the superposition principle, the mechanical model of the full-length bonded prestressed bolt and the theoretical calculation formula of the axial force and shear stress are given. The numerical simulation results extend the research depth of full-length bonded prestressed bolts and improve the theoretical system. However, due to the above limitations, it was determined that the reliability of the numerical simulation results can only be guaranteed when the anchor bolt only experiences axial deformation, and the accuracy and stability of the calculation method built in the simulation software were not taken into account.

7. Summary and Conclusions

(1) Different design parameters have different degrees of influence on the mechanical properties of the bolt. The bonding stiffness largely determines the peak axial force, peak interfacial shear stress, and number of sliding elements. Moreover, prestress had a significant impact on the peak axial force and the distribution of shear stress in the initial bonding section, while the length of the initial bonding section had a significant impact on the number of sliding elements and the peak axial force after sliding.

(2) The Grey correlation method was adopted to show that the correlation degrees of the design parameters of the initial bond segment, prestress, and bond stiffness was 0.8932, 0.9023, and 0.9775, respectively, that is, bond stiffness had the greatest influence, followed by prestress, and initial bond segment had the least influence.

Author Contributions: Conceptualization, F.S., Z.Z. and X.W.; methodology, F.S. and X.W.; data curation, K.Y. and X.G.; software, F.S. and K.Y; validation, Z.Z. and P.Z.; formal analysis, M.D., C.Y and P.Z.; writing—original draft preparation, F.S. and Z.Z.; writing—review and editing, Z.Z., F.S. and C.Y.; All authors have read and agreed to the published version of the manuscript.

Institutional Review Board Statement: Not applicable.

Informed Consent Statement: Not applicable.

Data Availability Statement: All relevant data are within the paper.

Conflicts of Interest: The authors declare no conflict of interest.

Appendix A

```
def tuomao
while_stepping
p_s = s_head
loop while p_s # null
c_cid = s_cid(p_s)
if c_cid >= 74
if c_cid <= 90
if sc_grslip(p_s,1) = 1
if sc_grslip(p_s,2) = 1
sc_grcoh(p_s) = 0
sc_grk(p_s) = 0
sc_grfric(p_s) = 0
end_if
end_if
end_if
end_if
p_s = s_next(p_s)
end_loop
end
@tuomao
```

References

1. Kang, H.P. Development and application of pre -stress anchored bolt supporting technology in coal mine. *Coal Min. Technol.* **2011**, *16*, 25–30.
2. Lin, J.; Wu, Y.; Ding, J.; Yang, J.; He, J. Optimization of bolt rod material used in rock-burst roadway bolting. *J. Coal* **2016**, *9*, 552–556. [CrossRef]

3.   Luo, J.; Peng, Z.; Wang, X.; Yan, Z.; Lin, J.; Liu, L. Mechanical behavior of novel basalt fiber-reinforced polymer (BFRP) rock bolt. *J. Compos. Mater. Sci. Eng.* **2022**, *347*, 79–86. [CrossRef]

4.   Feng, J.; Wang, Y.; Wu, H.; Lai, B.; Xie, X. Field pullout tests of basalt fiber-reinforced polymer ground anchor. *Rock Soil Mech.* **2019**, *40*, 2563–2573. [CrossRef]

5.   Liu, H.; Yu, X.; Li, G. Experimental study on tensile mechanical properties of glass fiber reinforced plastic rebar. *Chin. J. Rock Mech. Eng.* **2005**, *24*, 121–125. [CrossRef]

6.   Tao, Z.; Guo, A.; Zhang, J.; Xia, M.; Li, M.; Zhu, Z. How high tides, vessel, Static characteristics and engineering applications of micro negative Poisson's ratio bolt. *Rock Soil Mech.* **2022**, *43*, 808–818. [CrossRef]

7.   Zha, W.; Wang, C.; Liang, Y.; Liu, X.; Liu, Z. Experimental study on anchorage performance of new tension dispersed twist bolt. *Chin. J. Undergr. Space Eng.* **2022**, *18*, 696–701.

8.   Wang, B. Numerical Simulation of Supporting Effect of Anchoring Length on Roadway Surrounding Rock. Doctoral Thesis, Anhui University of Science and Technology, Huainan, China, 2015.

9.   Li, Y.; Zhao, C.; Cong, L.; Meng, X.; Dong, C. Analysis of stress distribution characteristics of fully anchored bolt based on actual surrounding rock deformation. *J. China Coal Soc.* **2019**, *44*, 2966.

10.   Wu, Y. Application study on prestressed full length bolting powerful support system. *Coal Sci. Technol.* **2011**, *39*, 27–30, 35.

11.   Wei, S.; Gou, P. Analogy simulation test on strengthening effect for pretention of bolts on anchorage body. *J. China Coal Soc.* **2012**, *37*, 1987–1993.

12.   Huang, M.; Lu, C.; Du, Y.; Tan, X. Nonlinear analysis on mechanical behavior of fully grouted bolts in tunnels due to surrounding rock deformation. *J. Saf. Environ.* **2022**, *22*, 2508–2513. [CrossRef]

13.   Zheng, X. Determination method and application of preload of full-length anchorage prestressed anchor bolt. *Min. Res. Dev.* **2015**, *35*, 60–63.

14.   Ding, X.; Gu, S.; He, H.; Zhang, Y. Force characteristic analysis of bolt under single and multiple bed separation. *Rock Soil Mech.* **2019**, *40*, 4299–4305.

15.   Li, C.; Stillborg, B. Analytical models for rock bolts. *Int. J. Rock Mech. Min. Sci.* **1999**, *36*, 1013–1029. [CrossRef]

16.   Das, K.; Sekhar, G.P.R.; Deb, D.; Narang, A. Analytical model for fully grouted rock bolts with multiple joints. In Proceedings of the 13th ISRM International Congress of Rock Mechanics, Montreal, QC, Canada, 10–13 May 2015.

17.   Li, J.; Zeng, H.; Yang, Z.; Lin, Z.; Chen, C. Analysis of bearing distribution on characteristics of pre-stressed end anchor after full anchorage. *China Min.* **2022**, *31*, 146–152.

18.   Du, Y.; Feng, G.; Kang, H.; Zhang, Y.; Zhang, X. Investigation on the pull-out bearing characteristics of bolts with different bond lengths. *J. Min. Strat. Control. Eng.* **2021**, *3*, 5–12. [CrossRef]

19.   Wang, X.; Yang, J.; Li, J.; Yang, L. Analysis of mechanical properties of fully-grouted bolts considering de-bonding under typical conditions. *J. Coal* **2020**, *S2*, 599–608. [CrossRef]

20.   Wang, X.; Kang, H.; Zhao, K.; Liu, Y. Numerical analysis of bonding stiffness for support effectiveness of pre-stressed bolts. *J. Coal* **2016**, *9*, 2999–3007. [CrossRef]

21.   Wang, Q.; Li, N.; Ye, H.; CHI, X.; Lei, T.; Chen, D. Study of failure characteristic and bolt's loading law of anchorage body with single face under uniaxial compression. *J. Min. Saf. Eng.* **2020**, *37*, 665–673.

22.   Gu, S.; Ding, X. The analysis of end anchoring-grouting prestressed anchor loading and support design with bed separation considered. *J. Min. Saf. Eng.* **2015**, *32*, 760–764.

23.   Yang, H.; Feng, X.; Yan, S. Experimental research on full-length anchoring system based on a new type of cement based material. *Saf. Coal Mine* **2021**, *52*, 89–94, 101.

24.   Feng, X. Failure Mechanism and Durability Exploration for Fully Bonded Bolting System. Doctoral Thesis, China University of Mining and Technology, Xuzhou, China, 2017.

25.   Gu, S.; Chen, X.; Ye, G. Stress distribution of anchorage section of prestressed rock bolt considering the shearing slip effect of grout-rock interface. *Min. Res. Dev.* **2010**, *30*, 34–36, 93.

26.   Song, Y.; Li, Y.; Du, Y. Variation of prestress loss of anchor rods under shear creep of jointed rock mass. *Rock Soil Mech.* **2020**, *S2*, 1–11.

27.   Lin, Q.; Qu, Z.; Guo, T.; Wang, Y. Factors Affecting Acid-etched Conductivity Based on Grey Correlation Method. *Sci. Technol. Eng.* **2019**, *19*, 106–110.

28.   Khalid, H.M.; Ojo, S.O.; Weaver, P.M. Inverse differential quadrature method for structural analysis of composite plates. *Comput. Struct.* **2022**, *263*, 106745. [CrossRef]

29.   Kabir, H.; Aghdam, M.M. A generalized 2D Bézier-based solution for stress analysis of notched epoxy resin plates reinforced with graphene nanoplatelets. *Thin-Walled Struct.* **2021**, *169*, 108484. [CrossRef]